Fatigue crack initiation and growth in a 35CrMo4 steel investigated by infrared thermography

O. PLEKHOV[2], T. PALIN-LUC[1], N. SAINTIER[1], S. UVAROV[2] and O. NAIMARK[2]

[1]E.N.S.A.M. CER de Bordeaux, Laboratoire Matériaux Endommagement Fiabilité et Ingénierie des Procédés (LAMEFIP), EA 2727, Esplanade des Arts et Métiers, 33405 Talence Cedex, France, [2]Institute of Continuous Media Mechanics RAS, 1 Koroleva str., 614013 Perm, Russia

ABSTRACT The present work is devoted to the investigation of fatigue crack initiation and growth in middle-cycle fatigue ($\sim 10^5$ cycles). Smooth specimens made of 35CrMo4 quenched and tempered steel were loaded in fully reversed plane bending. Temperature field evolution in time was recorded with an infrared camera. The experimental results show that the local heating of metal under fatigue loading is a sensitive and accurate enough manifestation of small fatigue crack initiation. It is shown that the time evolution of the spatial standard deviation of the temperature field can be used to investigate the damage localization and to monitor both the crack initiation and the current location of the fatigue crack tip. This should help to investigate the behaviour of defect during cyclic loading.

Keywords crack growth; crack initiation; infrared thermography; middle-cycle fatigue.

INTRODUCTION

The evolution of microstructure in metallic materials under cyclic loading has been the object of intensive studies during the last century. It has been shown that the fatigue of metal is accompanied by the appearance of specific dislocation patterns such as veins or channel structures, persistent slip bands-matrix structures, labyrinths or shell structures.[1] This evolution simultaneously involves a great number of strong nonlinear interactions of defects at different scales. These phenomena lead to a specific change of the macroscopic material response.

The description of these interactions requires both detailed theoretical investigation of the nonlinear laws of defect kinetics and the development of new experimental techniques. Based on the statistical physics approach, Naimark proposed a powerful way[2] to obtain the nonlinear kinetic equations for defect density. To progress in the development of this approach and to identify additional constants in the constitutive equations, a detailed investigation of the processes of plastic deformation, damage and failure is strongly needed.

Any phenomenon of localization, for example, plastic deformation in persistent slip bands or damage localization such as fatigue crack initiation, induces a heterogeneous distribution of heat sources on the surface of a specimen that makes it interesting to investigate the infrared radiation from the surface. In recent years, progress in the development of new infrared cameras allows us to use infrared thermography as a powerful, non-destructive and non-contacting technique for the investigation of the fatigue behaviour of materials.

First, observations of temperature evolution by different experimental techniques are presented in Refs [3] and [4]. It was shown that infrared thermography could be considered as an efficient way to estimate the fatigue properties of materials and structures. A technique for a fast estimation of the endurance limit of metals was proposed in 1986 and called the Risitano's technique.[5,6] This approach was also applied by Luong[7] and Blarasin *et al*.[8] Then, it has been developed to determine the whole *S–N* curve.[9]

Differential infrared thermography was also used successfully to estimate the value of the stress intensity factors.[10,11] This technique was adopted for fatigue crack tip localization and stress intensity factor estimation in Refs [12] and [13] based on the idea proposed in Ref. [11].

The present work is devoted to the investigation in middle-cycle fatigue (around 10^5 cycles) of the temperature heterogeneity, appearing with fatigue crack initiation, at the surface of smooth specimens made of 35CrMo4 quenched and tempered steel. The aim of this paper is to find an appropriate technique for detecting in space and in time the plastic strain localization, initiation and propagation of small fatigue cracks by monitoring the

Correspondence: Thierry Palin-Luc. E-mail: thierry.palin-luc@lamef.bordeaux.ensam.fr

characteristics of the temperature field on the specimen free surface.

EXPERIMENTAL PROCEDURE

Material and specimen

The material investigated is 35CrMo4 quenched and tempered steel, which has been already studied by Vivensang.[14] Its chemical composition is given in Table 1. The heat-treatment procedure before specimen machining was as follows: 30 min at 850 °C, then quenched in oil, then 1 h at 550 °C, and then left in air to cool. After this treatment, the mean grain size was around 10 μm.[14] The microstructure consisted of fine tempered martensite. The mechanical properties of this steel under quasistatic monotonic tension are given in Table 2.

The specimens used to carry out the fatigue tests were machined from round heat-treated bars (external diameter 26 mm) and their geometry is illustrated in Fig. 1. The theoretical stress concentration factor, K_t, of these smooth specimens in bending is 1.05.[15] Before experiments, all the specimens were polished with emery paper and diamond powder up to grade 1 μm. All the fatigue tests were carried out in fully reversed sinusoidal plane bending with a resonant electrodynamic fatigue testing machine designed at ENSAM-LAMEFIP. The loading frequency was 56 Hz. The tests automatically stopped when the loading frequency decreased to more than ~10% of the initial resonant frequency (undamaged specimen). This corresponded to a fatigue macrocrack size of several millimetres in depth.

Table 1 Chemical composition of the 35CrMo4 steel studied (wt%)

C	Mn	Si	S	P	Ni	Cr	Mo
0.37	0.79	0.30	0.010	0.019	<0.17	1.00	0.18

Infrared (IR) recording conditions

During the fatigue tests, an infrared camera (CEDIP Jade III MWR) was used to record the temperature field evolution on the specimen surface. The main technical characteristics of this camera are as follows: spectral range 3–5 μm, maximum picture size* 320 × 240 pixels, maximum framing rate† 500 Hz, NETD‡ < 25 mK at 300°K and digital conversion** 14 bits. To increase the surface emissivity properties, the specimen surface was painted in black (matt paint) after polishing. The lenses of the IR camera were not located exactly perpendicular to the specimen surface. Indeed, to avoid any parasitic reflections coming from the specimen surface, the IR camera was located so that there was a small angle (a few degrees) between the normal vector to the specimen surface and the camera axis. Furthermore, a matt black piece of material was put over and all around the setup (Fig. 2) to reduce artefacts due to external radiative heat sources. The concave surface of the specimen given in Fig. 1 was observed with the IR camera. Because of the large radius ($R = 40$ mm), the theoretical stress concentration factor is close to one; thus the normal stress distribution is almost uniform on the area monitored on this face. The duration of each experiment presented hereafter was between 20 and 25 min. During this short duration, the room temperature changed very slowly and with a low magnitude range (<0.5 °C). For longer tests, it is necessary to use an unloaded reference specimen located close to the tested one. All the IR data presented in this paper were recorded with the synchronized mode of the camera. It means that all the pictures of a film were recorded when the bending moment was maximum.

Treatment of IR data

Damage localization and fatigue crack initiation should be accompanied by a non-uniform temperature field at the specimen surface. This property was investigated by computing the spatial standard deviation of the temperature (SDT) field using the following procedure.

Table 2 Mechanical properties of the quenched and tempered 35CrMo4 steel

Young modulus, E (GPa)	Yield stress, $Re_{0.2}$ (MPa)	Maximum tensile strength, R_m (MPa)	Endurance limit for 10^7 cycles (MPa)	Fatigue limit for 10^5 cycles (MPa)	Elongation after fracture A% (%)
200	950	1068	525	660	11.5

*The size of the corresponding image region on the specimen is dependent on the camera lens. Two lens are now available in our laboratory for the IR camera: the first with a focal distance of 50 mm has a spatial resolution of 0.14 mm for a specimen at 200 mm, the second with a magnification (x1) has a special resolution of 25 μm, the picture size is around 9 mm × 7 mm.

†Maximum frequency to take IR pictures (the shortest delay between two IR picture is 1/500s).

‡NETD: Noise Equivalent Temperature Difference. This is the thermal resolution, i.e. the smallest temperature difference which can be measured without numerical treatment like the mean value.

**Number of bits used to digitalize the thermosignal.

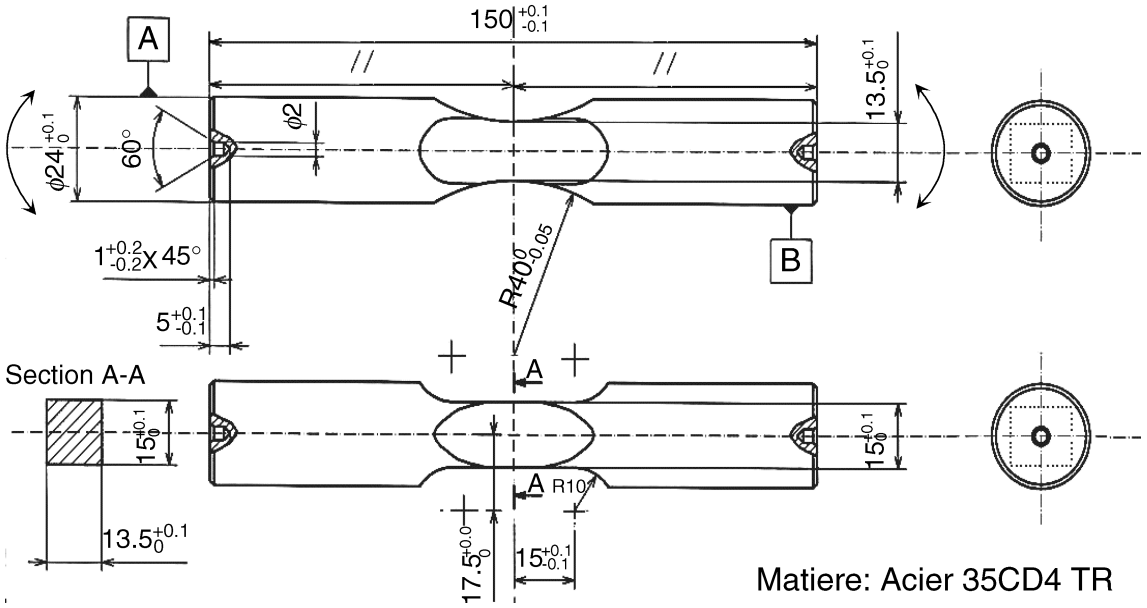

Fig. 1 Specimen geometry (arrows indicate plane bending moments; sizes in mm).

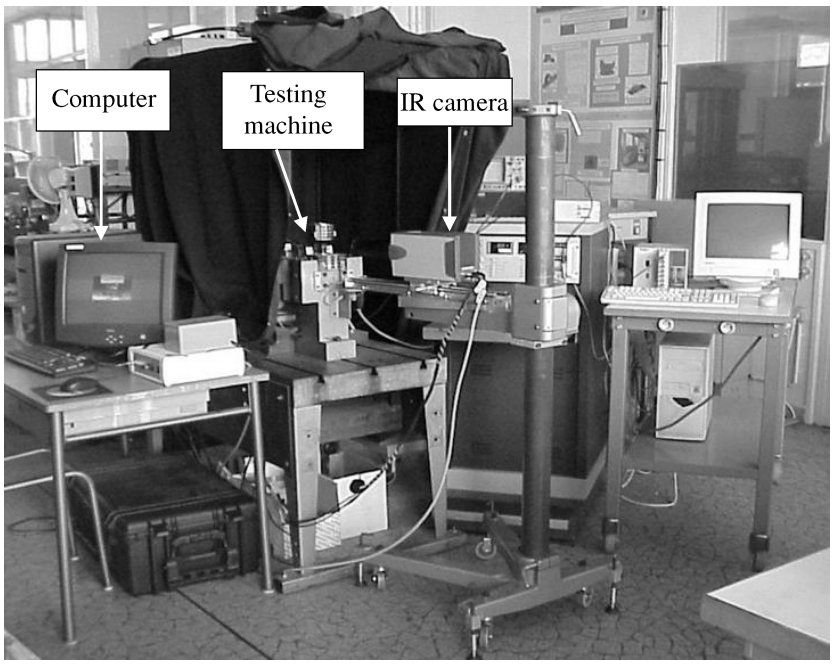

Fig. 2 Fatigue testing machine and IR camera with the matt black material removed to show the setup.

The IR data were treated *a posteriori*, i.e. after the fatigue test, when macrocrack initiation had been detected by the resonance frequency drop of the testing machine. Several Ω_j spatial areas were chosen such that each area contained several points $Z(x_i, y_i)$ (pixels—from 9 to 100—on the picture) where the temperature was known at each time t_k. This thermo-signal can be written as the sequence:

$$T(t, Z) = \{T(t_1, Z), T(t_2, Z), \ldots, T(t_k, Z), \ldots, T(t_N, Z)\}.$$

The Standard Deviation of Temperature in Ω_j, denoted by SDT_{Ω_j}, was computed through Eq. (1) by employing the IR experimental data obtained for the N_p points in Ω_j[16] (observation window of the IR camera projected on the specimen surface):

$$\mathrm{SDT}^2_{\Omega_j}(t_k) = \frac{1}{N_p - 1} \sum_{Z \in \Omega_j} \left(T(t_k, Z) - \bar{T}_{\Omega_j}(t_k)\right)^2, \qquad (1)$$

where $\bar{T}_{\Omega_j}(t_k) = \frac{1}{N_p} \sum_{i=1}^{N_p} T(t_k, Z(x_i, y_i))$ is the spatial mean value over Ω_j of the temperature at time t_k. An example

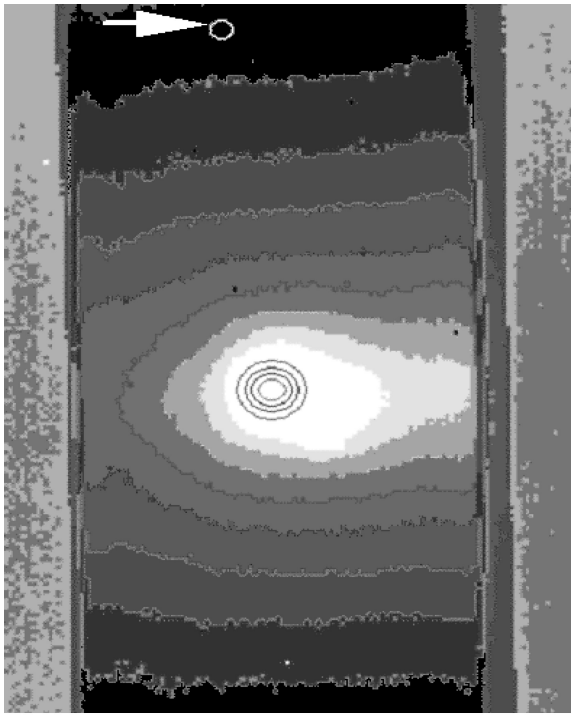

(a)

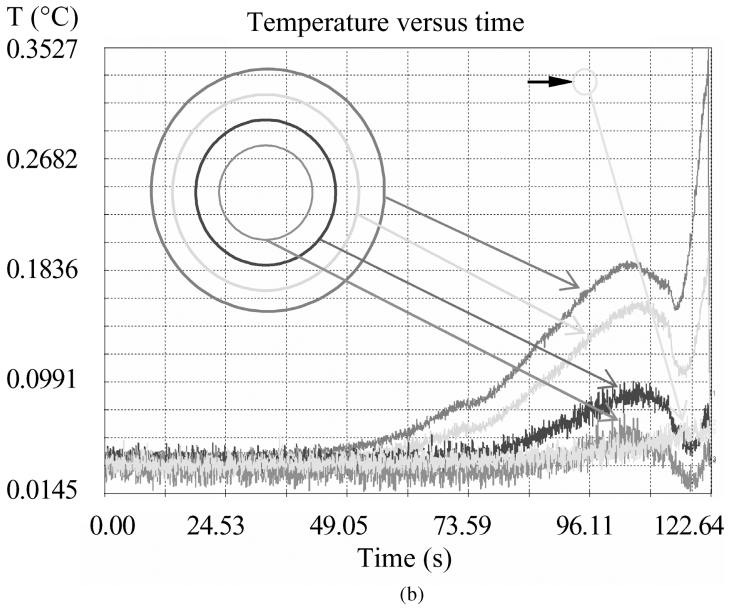

(b)

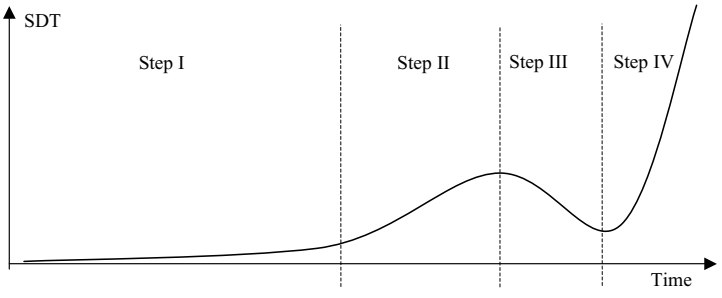

(c)

of five spatial areas (Ω_1 to Ω_5 areas) is shown in Fig. 3 with typical temporal evolution of the standard deviation SDT. These areas are defined by four circles around the hot spot with the following diameters: 0.6, 1, 1.5, 2 and 2.5 mm, and one circle far from the hot spot (top of the picture Fig. 3a).

EXPERIMENTAL RESULTS

Figure 3 shows the evolution of the SDT as a function of time during the last 123 s of a specimen life (loaded at a stress amplitude of 650 MPa; the total life is 83 300 cycles or ~1500 s) for five different area sizes. For the four curves related to the four areas around the hot spot (circles in the middle of Fig. 3a) the peak shape is the same. The shape of the curves tends to a common smooth curve (without any peak) elsewhere (far from the hot spot) as illustrated by the curve in Fig. 3b related to the small area (circle) at the top of Fig. 3a. Four main steps with two knee points can be identified as illustrated in Fig. 3c:

- Step I : The SDT is stable, the temperature field is homogeneous, independent of the area of investigation.

Fig. 3 (a) Temperature pattern. (b) SDT evolution versus time for five different areas. (c) Schema of the four different stages.

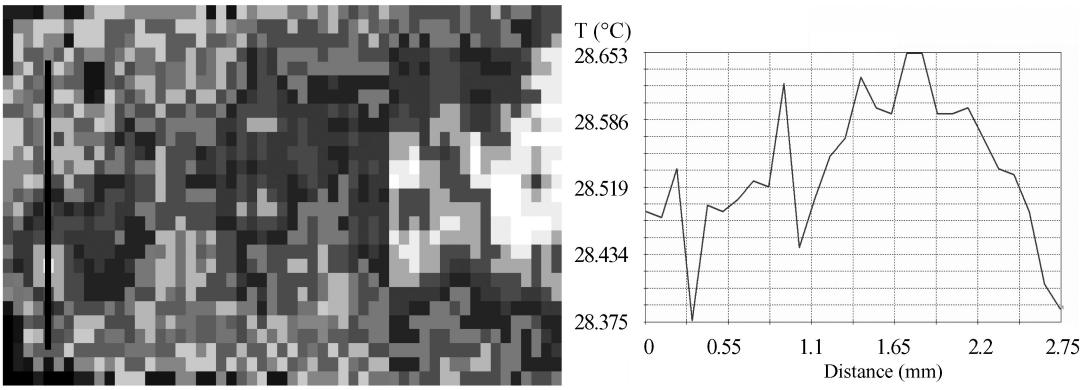

(a) *Crack initiation, N=80 830 cycles (≈ 1443 s). White pixels are an artifact due to the small angle between the axis of the camera lens and the specimen surface.*

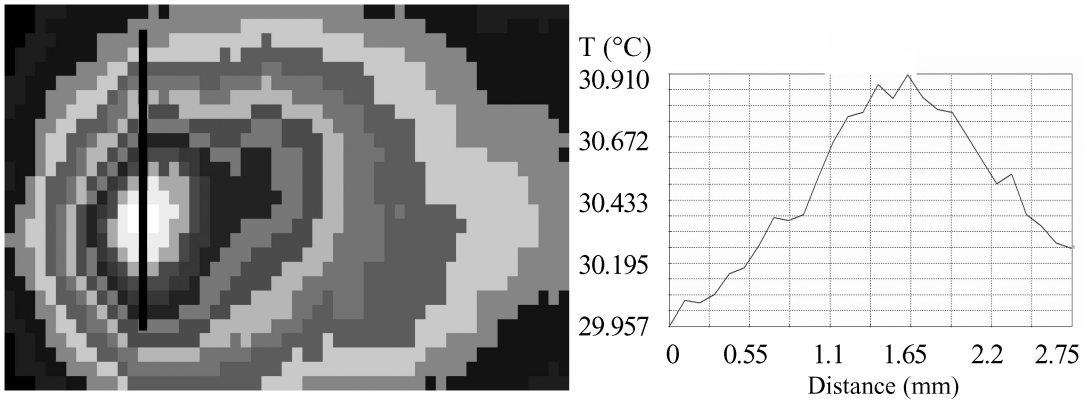

(b) *Crack propagation, N=82 550 cycles (≈ 1474 s).*

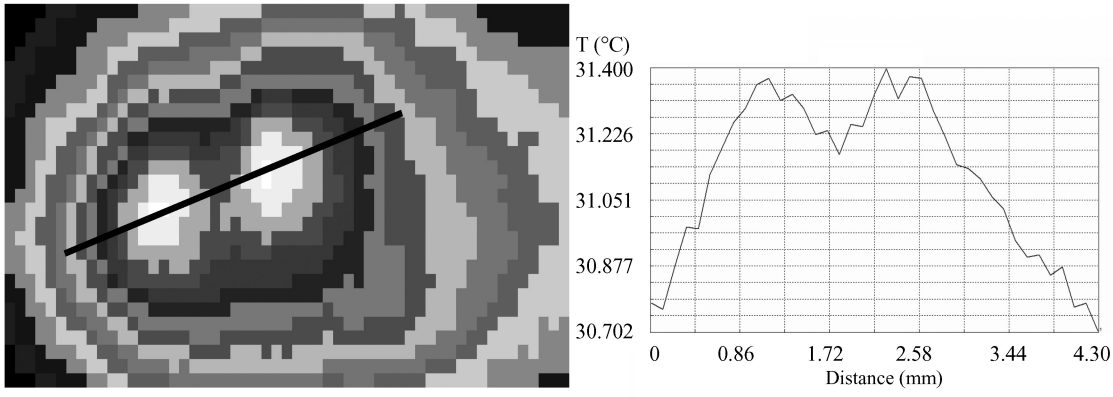

(c) *Crack jumping, N=82 785 cycles (≈1478 s).*

Fig. 4 Close up pictures of damage localization (left) and the cross section of the temperature field in the hottest points (right).

- Step II : The SDT increases markedly. A heterogeneous temperature field takes place. The magnitude increase of SDT depends on the area of investigation.
- First knee point.
- Step III : Simultaneous drop of the SDT in all areas.
- Second knee point.
- Step IV : Sudden and sharp increase in the SDT.

It has to be noticed that the first knee point is observed before the sharp change in the resonance frequency of the fatigue testing machine. The knee-point shape of this curve is discussed in detail later. Nevertheless, one can say that this phenomenon identifies the beginning of the correlation behaviour between the adjacent points in the temperature field and the thermal behaviour of the hot

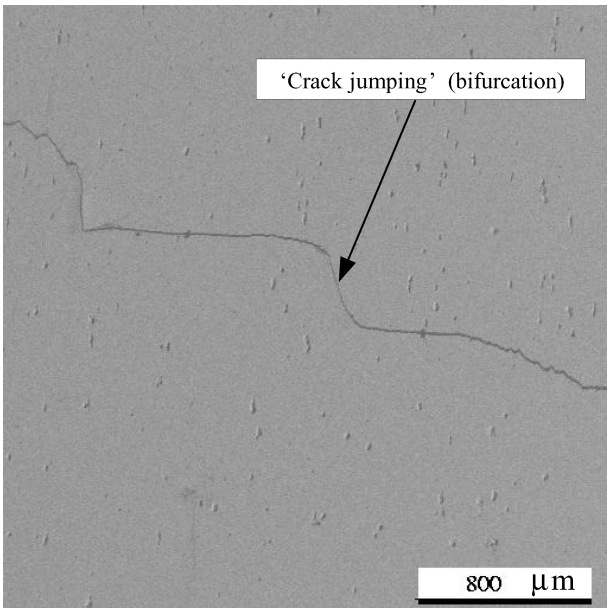

Fig. 5 SEM image of a 'crack jump' (bifurcation) as seen in the IR image in Fig. 4.

spot. Indeed, SDT is nothing else but a measure of the difference between the thermal behaviour of each pixel and the mean value of the temperature field over all the investigated area. One can suggest that the collective behaviour of the points is the consequence of small fatigue crack initiation in the investigated area. It is useful to discuss this in the study of the temperature pattern evolution.

Figure 4 presents several frames from the last 2500 cycles of an experiment at a stress amplitude of 650 MPa (this stress exceeds the endurance limit of the material). The total lifetime was 83 300 cycles up to the automatic detection of a macrocrack by the testing machine. The size of the area investigated was 2.8 × 5.5 mm. The pictures on the right in Fig. 4 are the cross sections of the temperature profile along the lines drawn in the left-hand pictures. The temperature distribution allows us to conclude that we observe the initiation (a), propagation (b) and jump (c) of a fatigue crack. More precisely, the process is called 'crack jump' when a hot spot corresponding to the current crack tip stops, and a second hot spot is detected at a short distance (about 1 mm). Then the temperature of

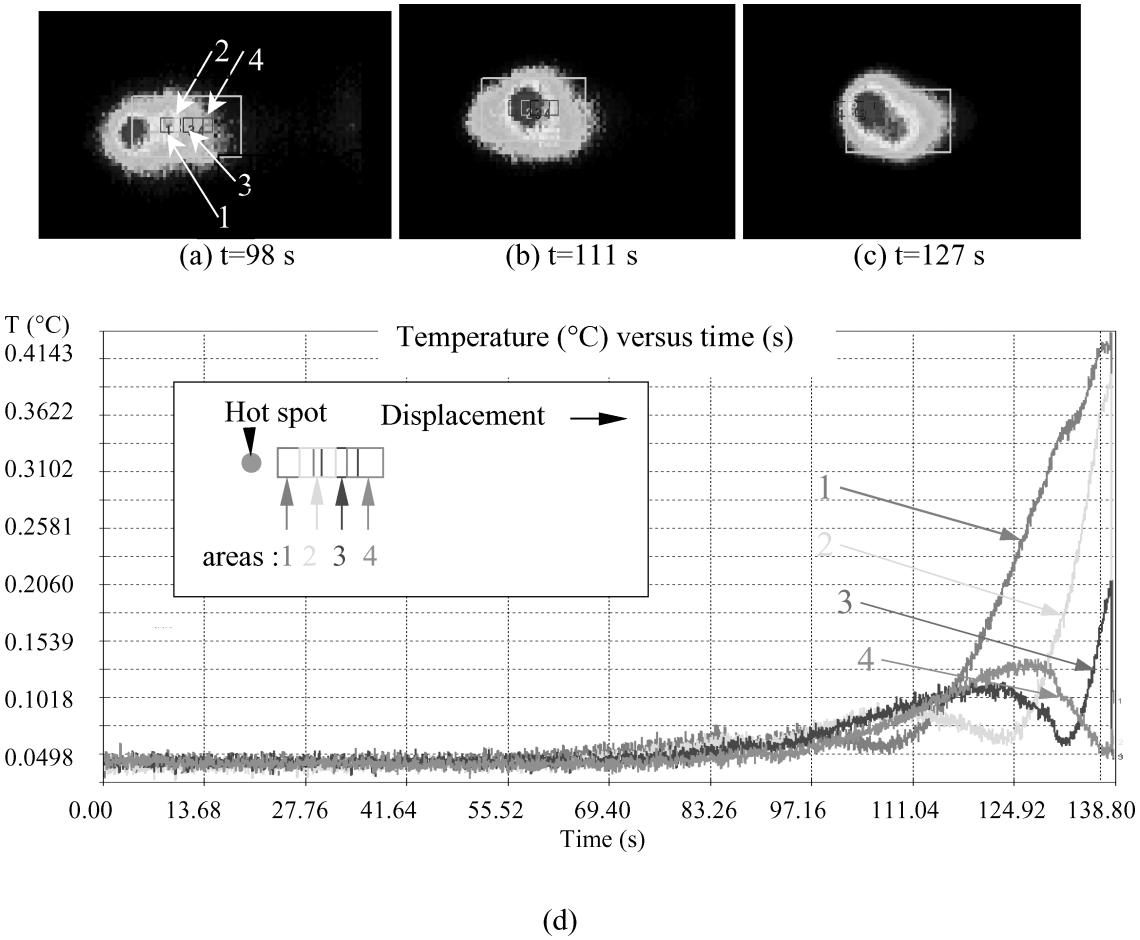

Fig. 6 Location of hot spot (a, b, c) and the corresponding temporal evolution of the standard deviation of temperature (d).

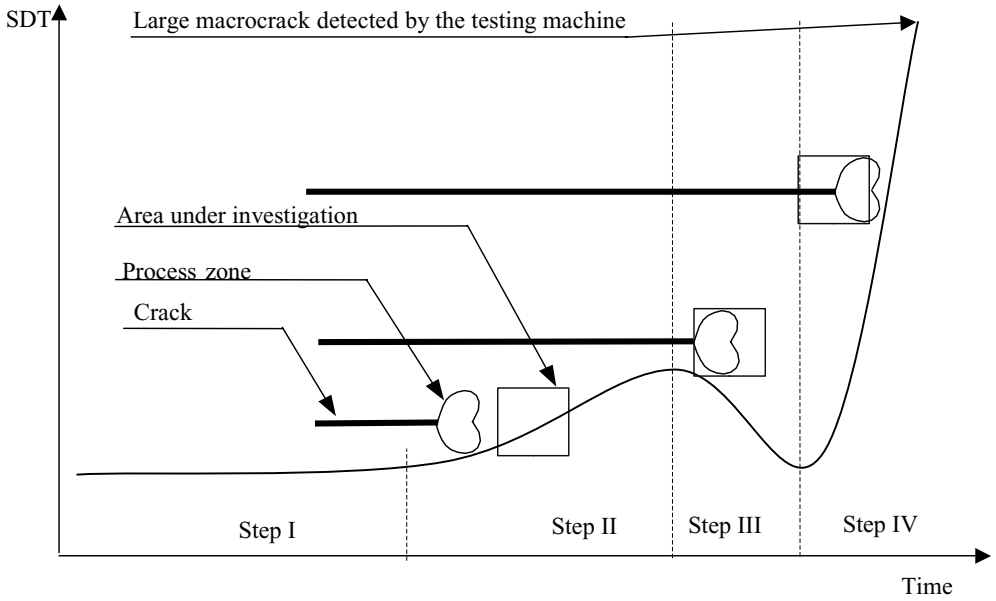

Fig. 7 Schema of the fatigue crack and process zone location, the investigated area and the SDT temporal evolution.

the first spot decreases and the temperature of the second one increases, as is shown in Fig. 4c. The crack path with the crack jump, corresponding to the IR picture in Fig. 4c, is illustrated by the SEM picture in Fig. 5.

To clearly illustrate a connection between the SDT evolution versus time and the position of the Ω area under investigation, four areas (small rectangles) were located as shown in Fig. 6, and the temporal evolution of the SDT in these zones was analysed. These areas are on the right-hand side of the crack tip, which is moving from the right to the left through the four areas. The picture represents the last 140 s (7840 cycles) of the specimen life. Before this period, we could not detect significant changes in the slope of the SDT curve.

The arrangements of small areas in Figs 6a–c were fixed in space, and the analysis allows the following conclusions as illustrated with a schema in Fig. 7:

- When there is no fatigue crack, the SDT is very low and stable (the temperature field is homogeneous).
- The SDT increase (Step II) can be due to two phenomena: fatigue crack initiation in the area investigated or crack propagation of an existing crack towards this area.
- An SDT decrease (Step III) is observed when the area of observation is smaller than the hot-spot size, and/or when the entire process zone in front of the crack tip is inside the investigated area.
- The SDT sharply increases when the crack-tip propagates outwards the area investigated.

In order to give a better understanding of the connection between the current crack-tip position and the SDT evolution, a one-dimensional analysis is presented in the following section.

DISCUSSION

As a result of our investigation, infrared thermography seems to be a promising technique for detecting fatigue crack initiation and monitoring fatigue crack tip location. But the most interesting question is related to the smallest size of detectable defect. We can reformulate this question as: Is it possible to use the infrared thermography as a technique for the prediction of fatigue crack initiation through the detection of fatigue crack precursor?

To answer this question and to justify our previous explanations, let us consider a one-dimensional problem consisting of a hot spot centred at x_0 abscissa according to Eq. (2):

$$T(x,t) = T_\alpha + T_\beta(t)\mathrm{Exp}\{-[x - x_0(t)]^2\}. \quad (2)$$

This hot spot is characterized by $\delta(t)$: the full width at half maximum of the function given equation (2). $\delta(t)$ is so that $\delta(t) = b(t) - \mathrm{a}(t)$ where $T(a,t) = T(b,t) = \max_x[(T(x,t)]/2$, and $a \neq b$. In our case $\delta = 2\sqrt{\ln(2)}$, and is time independent. It is assumed now that this hot spot is moving, as a stable fatigue crack, while the observation window is fixed in time. In the first approximation, the hot spot centre displacement is assumed to be linear (left-hand side of Eq. (3)). The stress increases at the crack tip due to the crack growth and, as a consequence of thermoelasticity, the temperature also increases. In order to observe the effect of a temperature increase on the SDT, the temperature rise is considered

to evolve linearly with time (very slowly), as is described by Eq. (3):

$$x_0(t) = x_{01} + \dot{x}_0 t \text{ and } T_\beta(t) = T_{\beta_0} + \alpha t. \quad (3)$$

The temperature field (one dimension here) is then observed in a window limited by the [a,b] segment centred in $c = (a+b)/2$ and of width $l = (b-a)$. From Eqs (2) and (3), the mean temperature and SDT computed over [a,b] are given in Eqs (4) and (5), respectively:

$$\bar{T}(t) = T_\alpha(t) + \frac{T_\beta(t)}{b-a}\left[\frac{\sqrt{\pi}}{2}\mathrm{Erf}(a - x_0(t); b - x_0(t))\right] \quad (4)$$

$$\mathrm{SDT}^2 = \frac{\sqrt{\pi}T_\beta(t)^2}{2l}[\mathrm{Erf}(a - x_0(t); b - x_0(t))] - \frac{\pi T_\beta(t)^2}{4l^2}[\mathrm{Erf}(a - x_0(t); b - x_0(t))]^2, \quad (5)$$

where $\mathrm{Erf}(u;v) = \frac{2}{\sqrt{\pi}}\int_u^v \exp(-x^2)\,\mathrm{d}x$.

Figure 8 shows the evolution of the normalized SDT (i.e. SDT/$T_{\beta 0}$) as a function of the window width, for a fixed hot spot in position and in time and a centred window ($T_\beta(t) = T_{\beta_0},\ x_0(t) = \mathrm{x}_0$). It shows that the sensitivity of SDT is maximum when the observation window width is equal to approximately three times the full width half maximum of the hot spot. This means that for practical applications, the observation window should not be too small but proportionate to the hot-spot sizes to be measured. In our case, typical hot-spot sizes are of approximately 1 mm (hot spots are not very sharp due to heat conductivity), thus the observation window width has to be equal to approximately 3 mm.

Figure 9 shows the influence of the window width l on the SDT evolution when the hot spot evolution is described by Eqs (2) and (3). According to this figure, the shape of the SDT versus time curves is independent of the window width, as is also observed in experiments in Fig. 3b. In our simulation, the first knee point corresponds to the beginning of the hot spot coming into the observation window. One can notice that the minimum of each SDT(t) curve occurs at the same time. This corresponds to the

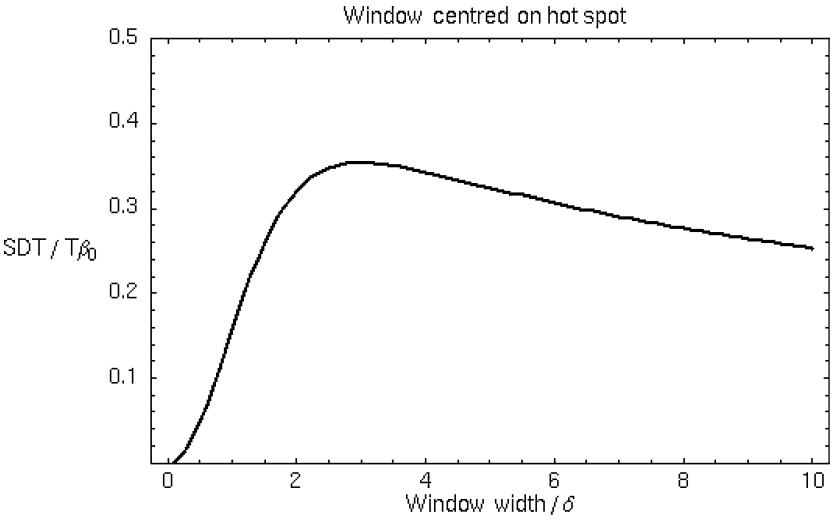

Fig. 8 Normalized SDT evolution versus relative window width for a window centred on the hot spot ($T_{\beta 0} = 1\ ^\circ\mathrm{C}$).

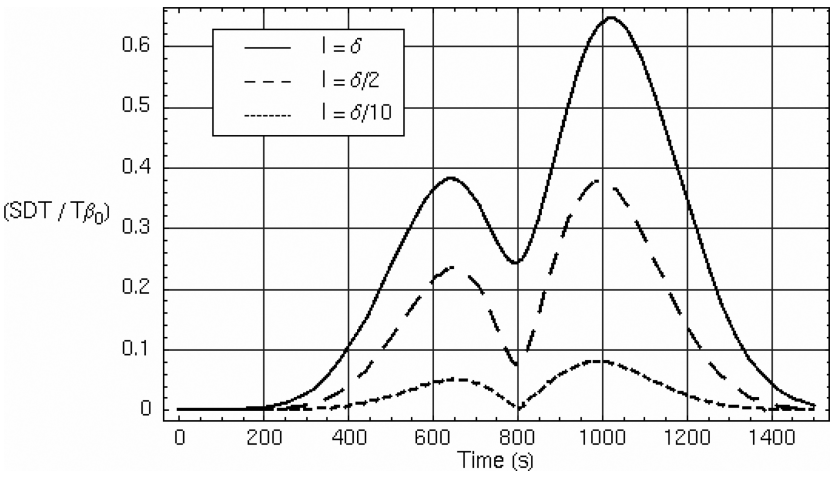

Fig. 9 SDT simulation of three different windows ($l = \delta$, $l = \delta/2$ and $l = \delta/10$) at the same location (with $\dot{x}_0 = \delta/400$, $T_\beta(t) = 0.001 + 0.001t$).

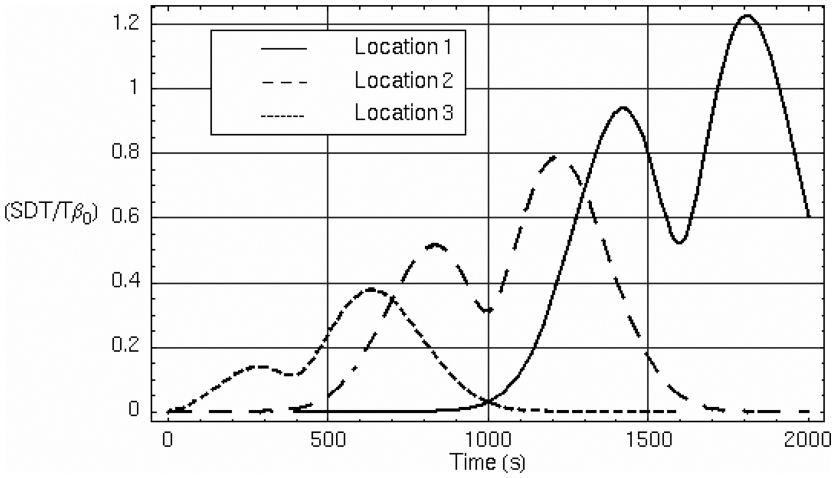

Fig. 10 SDT simulation of three different windows with the same width ($l = \delta$) and the distance between each centre equal to 1.5 δ (with $\dot{x}_0 = \delta/400$, $T_\beta(t) = 0.001 + 0.001t$).

instant at which the hot spot location coincides with the centre of the observation window.

The shape of the SDT simulation is in agreement with the observation up to the second increase just after the local minimum. In the experiments, the second maximum is not observed. One possible reason is that the one-dimensional simulation is too simple. Indeed, in practice, the temperature distributions behind and in front of the crack tip are very different. In particular, the presence of a material discontinuity (crack) behind the crack tip generates strong emissivity perturbations on the specimen surface. This induces discontinuities in the temperature field that create a very heterogeneous temperature field and is responsible for the sharp SDT increase.

Figure 10 illustrates the SDT simulation for three windows with the same width $l = \delta$, and the distance between each centre equal to 1.5 δ. The shapes of the SDT curves are identical to those of the observed curves shown in Fig. 6. The minimum of SDT(t) is appearing at three different instants showing that this technique could be used in future to measure—after a fatigue test—the mean crack tip (hot spot) velocity between different observation windows, even if the load history is random.

CONCLUSION AND PROSPECTS

In our tests on smooth specimens in 35CrMo4 steel, damage localization, fatigue crack initiation and jumping-like propagation have been observed using an infrared camera. An indicator has been proposed to monitor the crack initiation: the temporal evolution of the spatial SDT.

The SDT evolution has been correlated with some fatigue crack initiation and propagation features. It has been shown that a sudden increase of the SDT corresponds to crack initiation in the area investigated. This particular point could be used in the future to develop a new technique for real-time early detection of fatigue crack initiation. This will be possible when computer speeds are high enough to compute in real time the SDT(t) curves from the IR data, and compare them with a threshold value. Moreover, it has been proposed that the computation of the SDT evolution could be used to monitor fatigue crack propagation. This could be remarkably interesting in cases where other techniques, such as compliance or potential drop techniques, cannot be used.

Infrared techniques have been used by several authors[5–9] to estimate the fatigue limit and the endurance limit of metals. However, in order to progress our understanding of the influence of fatigue damage and fatigue crack initiation (linked with heat sources appearance) on the temperature field (analysed by IR thermography) on the specimen surface, further experimental investigations have to be carried out. They should couple the infrared monitoring and microstructural investigation of the specimen surface by using, for instance, interrupted fatigue tests and SEM observations. The theoretical study should also progress in the description of thermo-micromechanical process in the material and in the division of the energy absorbed by the specimen into two parts (heat dissipation and stored energy).

Such investigations could be useful to connect material defect evolution (persistent slip bands, intrusion–extrusion,...), such as predicted in Ref. [17], with local thermal non-uniformity. The main difficulty will be to distinguish data from experimental noise. The first attempt was done with a specific algorithm from chaos theory.[16]

Acknowledgements

This work has been carried out during the stay of Dr Plekhov at E.N.S.A.M.—LAMEFIP as post-doctoral student with the financial support of the French Ministry of Research. This Ministry is gratefully acknowledged for enabling the authors to do this work. Dr O. Plekhov also

acknowledges the Russian Science Support Foundation (grant for talented young researchers) for financial support for his research during his stay in Russia.

REFERENCES

1 Suresh, S. (1991) *Fatigue of Materials*. Cambridge University Press, Cambridge, UK.

2 Naimark, O. B. (1998) Instabilities in condensed media induced by defects. *JETP Lett.* **67**, 751–757.

3 Reifsnider, K. L. and Williams, R. S. (1974) Determination of fatigue related heat emission in composite materials. *Exp. Mech.* **14**, 479–485.

4 Reifsnider, K. L. and Stinchomb, W. W. (1976) *New Metods of Mechanical Materials Testing Using Termography*. Third Biennal Infrared Information Exchange, St. Louis, MO, 9–14.

5 La Rosa, G. and Risitano, A. (2000) Thermographic methodology for rapid determination of the fatigue limit of materials and mechanical components. *Int. J. Fatigue* **22**, 65–73.

6 Gurti, G., La Rosa, G., Orlando, M. and Risitano, A. (1986) Analisi framite infrarosso termoci della "temperature limite" in prove de fatica. In: *Proceedings of the 14th AIAS Italian National Conferenses*, Catania, Italy, pp. 211–220 (in Italian).

7 Luong, M. P. (1995) Infrared thermographics scanning of fatigue in metals. *Nucl. Engng Des.* **158**, 363–376.

8 Blarasin, A., Fracchia, R. and Pozzati, M. (1998) Valutazione rapida del limite di fatica di bielle motore in ghisa. *ATA Ingegneria Automotoristica* **51**, 255–265 (in Italian).

9 Fargione, G., Geraci, A., La Rosa, G. and Risitano, A. (2002) Rapid determination of the fatigue curve by the thermographic method. *Int. J. Fatigue* **24**, 11–19.

10 Stanley, P. and Chan, W. K. (1986) The determination of stress intensity factors and crack-tip velocities from thermoelastic infra-red emissions. *Proc. IMechE.* **C262**, 105–144.

11 Tomlinson, R. A., Nurse, A. D. and Patterson, E. A. (1997) On determining stress intensity factors for mixed mode cracks from thermoelastic data. *Fatigue Fract. Engng Mater. Struct.* **20**, 217–226.

12 Diaz, F. A., Patterson, E. A. and Yates, J. R. (2003) Fatigue crack growth analysis using TSA. In: *Proceedings of International Conference on Fatigue Crack Path*, ESIS, Parma, Italy.

13 Diaz, F. A., Patterson, E. A., Tomlinson, R. A. and Yates, J. R. (2004) Measuring stress intensity factors during fatigue crack growth using thermoelasticity. *Fatigue Fract. Engng Mater. Struct.* 7, 571–583.

14 Vivensang, M. (1994) Ph.D. Thesis. 'Comportement en fatigue de deux nuances d'acier 35CD4'. E.N.S.A.M., Bordeaux, France.

15 Peterson, R. (1974) *Stress Concentration Factors*. John Wiley and Sons-Interscience, New York.

16 Plekhov, O. A., Uvarov, S. V., Palin-Luc, T. and Naimark, O. B. (2003) Investigation of fatigue crack initiation and growth in 35CD4 steel by infrared thermography. In: *Proceedings of International Conference on Fatigue Crack Path*. ESIS, Parma, Italy.

17 Naimark, O. B., Davydova, M. M., Plekhov, O. A. and Uvarov, S. V. (1999) Experimental and theoretical studies of dynamic stochasticity and scaling during crack propagation. *Phys. Mesomech.* **2**, 43–53.